



Article

# Electromagnetic Effective Medium Modelling of Composites with Metal-Semiconductor Core-Shell Type Inclusions

Yael Gutiérrez, Dolores Ortiz, Rodrigo Alcaraz de la Osa, José M. Saiz , Francisco González and Fernando Moreno \* 

Department of Applied Physics, University of Cantabria, Avda. Los Castros s/n, 39005 Santander, Spain

\* Correspondence: morenof@unican.es

Received: 13 June 2019; Accepted: 18 July 2019; Published: 22 July 2019



**Abstract:** The possibility of using light to drive chemical reactions has highlighted the role of photocatalysis as a key tool to address the environmental and energy issues faced by today's society. Plasmonic photocatalysis, proposed to circumvent some of the problems of conventional semiconductor catalysis, uses hetero-nanostructures composed by plasmonic metals and semiconductors as catalysts. Metal-semiconductor core-shell nanoparticles present advantages (i.e., protecting the metal and enlarging the active sites) with respect to other hetero-nanostructures proposed for plasmonic photocatalysis applications. In order to maximize light absorption in the catalyst, it is critical to accurately model the reflectance/absorbance/transmittance of composites and colloids with metal-semiconductor core-shell nanoparticle inclusions. Here, we present a new method for calculating the effective dielectric function of metal-semiconductor core-shell nanoparticles and its comparison with existing theories showing clear advantages. Particularly, this new method has shown the best performance in the prediction of the spectral position of the localized plasmonic resonances, a key parameter in the design of efficient photocatalysts. This new approach can be considered as a useful tool for designing coated particles with desired plasmonic properties and engineering the effective permittivity of composites with core-shell type inclusions which are used in photocatalysis and solar energy harvesting applications.

**Keywords:** effective medium theory; metal-semiconductor; core-shell; photocatalysis; plasmonics

## 1. Introduction

The field of plasmonic photocatalysis has experienced a great development in the recent years [1–3] as a clean technique for solar energy conversion. It has arisen as an alternative to conventional semiconductor catalysis in order to overcome some of its drawbacks [2,3]. Semiconductor photocatalysis uses semiconductors to absorb light and create electron-hole pairs ( $e-h$ ) that can initiate reduction and/or oxidation chemical reactions. However, during this process, two main difficulties arise: low photocatalytic efficiency due to the  $e-h$  recombination, and the lack of high-performance photocatalytic materials with band gaps that can absorb visible light. For instance, high performing semiconductor photocatalysts, like  $\text{TiO}_2$  or  $\text{CeO}_2$ , absorb light in the near-ultraviolet hampering solar-light driven photocatalytic reactions. The inclusion of metallic nanoparticles into the semiconductor enable new paths to circumvent these problems. At the metal-semiconductor interface, a Schottky junction appears, creating an internal electric field that forces both  $e$  and  $h$  into different directions inhibiting their recombination. In addition, metallic nanoparticles (NPs) support localized surface plasmon resonances (LSPRs) that also bring some benefits. Although common metals used in plasmonic photocatalysis such as gold (Au) or silver (Ag) present LSPR visibly, they are able to drive a photocatalytic response of large-band gap semiconductors (e.g.,  $\text{TiO}_2$  or  $\text{CeO}_2$ ) through

a charge-transfer mechanism. It consists of the transfer of photo-excited electrons from the metal into the conduction band of the semiconductor [2,3]. LSPRs also create very strong electromagnetic fields confined in subwavelength dimensions at the vicinity of the nanoparticles, which can increase the  $e-h$  pair generation [2]. Moreover, the excitation of LSPRs in metals inherently produces heat due to Joule losses. This temperature increment increases redox reaction rates, mass transfer and polarizes nonpolar molecules for better absorption.

A lot of effort has been invested in the synthesis and design of metal-semiconductor photocatalysts. This includes choosing both the semiconductor and metal, and the configuration of the systems (size, shape, interface design, ...) [2,4]. Nanostructuring the metal-semiconductor system into nanoparticles has been widely studied as a way to boost the photocatalytic performance by increasing the surface-to-volume ratios. The synthesis of large variety of metal-semiconductor NPs has been reported in the literature e.g., metal-semiconductor core-shell NPs or semiconductor NPs with their surfaces decorated with metal inclusions [4,5]. Specifically, core-shell nanostructures present special advantages for photocatalytic reactions such as protecting the metal and enlarging the active sites [4]. These NP systems are usually supported in a host matrix or solvent. To maximize solar absorption, it is critical to accurately model the reflectance/absorptance/transmittance of the host-matrix with metal-semiconductor NPs as inclusions. In principle, these systems, assuming that the inclusions behave as electric dipoles, could be modeled using, for example, classical Maxwell Garnett effective medium theory (EMT) [6]. Maxwell Garnett EMT allows the calculation of the effective dielectric function of the host matrix with metal-semiconductor NPs inclusions taking as inputs the dielectric function of both the host and the inclusions. At this point, the problem arises regarding: *which is the dielectric function of the metal-semiconductor inclusion?* In this contribution, we propose a new procedure to calculate the effective dielectric function of metal-semiconductor core-shell NPs. In this way, we enable the use of Maxwell Garnett EMT or equivalent EMTs for the modeling of state-of-the-art plasmonic photocatalytic systems in which metal-semiconductor core-shell photocatalysts are supported in a matrix of arbitrary dielectric function [7,8]. Note that similar configurations are also widely used in solar energy harvesting applications [9–11]. This procedure is illustrated in Figure 1: the proposed approach is used to calculate the effective dielectric function of the core-shell inclusions  $\epsilon_{cs}$ . Then, the problem is reduced to the one of a matrix with spherical inclusions randomly distributed. This system is commonly solved by applying Maxwell Garnett EMT or equivalent EMTs; taking as input the effective dielectric function of the core-shell  $\epsilon_{cs}$  and the host matrix  $\epsilon_h$ , the effective dielectric function of the whole system  $\epsilon_{eff}$  is calculated. Therefore, the initial system (i.e., host material with core-shell inclusions) is reduced to a homogeneous medium with dielectric function  $\epsilon_{eff}$ .



**Figure 1.** Scheme of the effective medium problem of composite with spherical core-shell type inclusions: the system formed by a composite with core-shell inclusions can be reduced to that of a composite with homogeneous spheres with effective dielectric function  $\epsilon_{cs}$ . The value of  $\epsilon_{cs}$  is obtained by applying an effective medium theory on the core-shell inclusion.

The paper is organized as follows: first, we perform a detailed study on the effective medium theories used by other authors in the literature to model core-shell NPs. Secondly, we present the basis of the new EMT for core-shell NPs developed in this work. In the following section, and in order to validate our method, we compare the exact extinction efficiencies of different metal-semiconductor core-shell NPs calculated through Mie theory with that obtained by using the effective dielectric functions in Mie theory for a homogeneous sphere. Afterwards, we give an example about the

applicability of the proposed method developed here: the calculation of the reflectance of a composite with core-shell type inclusions. Finally, the main conclusions of this research are presented.

## 2. Effective Medium Theories

Although the electromagnetic response of spherical core-shell NPs has an analytical solution given by Mie theory [12], it is not trivial to obtain an effective dielectric function of this system. Mie theory for a coated sphere gives exact analytical expressions for the absorption/scattering/extinction efficiencies and scattered electric and magnetic fields. However, it does not provide an expression for the effective dielectric function of a coated sphere. Therefore, effective medium theories (EMTs) give an alternative to deal with this problem. EMTs allow us to obtain the dielectric function of an equivalent sphere with the same size and electromagnetic behavior as a given spherical core-shell NP. This process is illustrated in Figure 2.

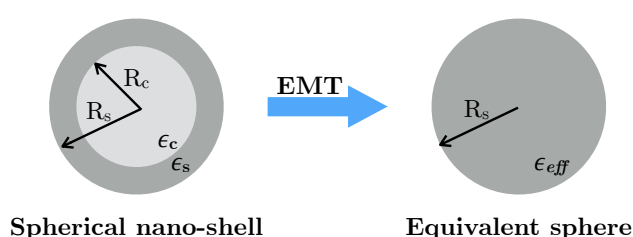


**Figure 2.** Scheme of the effective medium problem for a spherical nano-shell: a coated sphere of radius  $R_s$  formed by a core—dielectric function  $\epsilon_c$  and radius  $R_c$ —and a shell—dielectric function  $\epsilon_s$ —is reduced to a homogeneous sphere—radius  $R_s$ —applying an effective medium theory (EMT) to calculate its effective dielectric function  $\epsilon_{eff}$ .

Although in the literature several EMTs have been used to model the electromagnetic response of core-shell NPs [11,13–17], here we present a new approach that overcomes some of the limitations of the existing EMTs. Specifically, we compare the proposed approach with the weighted average, Bruggeman, Maxwell Garnett, Internal Homogenization and Mie theory based Maxwell Garnett.

In the following subsections, we will review the aforementioned EMTs, their limitations and their applicability to the proposed problem: *calculating the effective dielectric function of a metal-semiconductor core-shell spherical nanoparticles.*

### 2.1. Weighted Average (WA)

One of the simplest approaches to get the effective dielectric function ( $\epsilon_{eff}$ ) of a core-shell nanoparticle is given by the weighted average of the dielectric functions of both the core ( $\epsilon_c$ ) and the shell ( $\epsilon_s$ ),

$$\epsilon_{eff} = f\epsilon_c + (1 - f)\epsilon_s \quad (1)$$

where  $f = R_c^3/R_s^3$  is the fraction of volume that occupies the core. When  $f = 1$  (core-material particle),  $\epsilon_{eff} = \epsilon_c$ . Conversely, when  $f = 0$  (shell-material particle),  $\epsilon_{eff} = \epsilon_s$ . This approach has been used by Kuzma et al. [13] to model the effective dielectric function of Ag/Ag<sub>2</sub>O core-shell nano-spheres.

### 2.2. Bruggeman

Bruggeman's effective medium theory [12,18] is proposed for non-homogeneous media in which two materials are present, the main one—the matrix—hosting the secondary one—the inclusion. Both materials, however, are given the same importance, i.e., it is invariant to an interchange between the host matrix and the inclusions. In this approximation, the effective dielectric function  $\epsilon_{eff}$  is given by

$$f \frac{\epsilon_c - \epsilon_{eff}}{\epsilon_c + 2\epsilon_{eff}} + (1 - f) \frac{\epsilon_s - \epsilon_{eff}}{\epsilon_s + 2\epsilon_{eff}} = 0, \quad (2)$$

where  $\epsilon_s$  and  $\epsilon_c$  are the dielectric functions of the host (in our case the shell) and the inclusions (the core), respectively.  $f$  is the filling factor of the inclusions. If in Equation (2), we now consider the filling fraction of the host ( $f'$ ) instead of the one of the inclusion ( $f' = (1 - f)$ ), we obtain an equivalent expression. This means that which component is labelled as inclusion or host does not matter, both are interchangeable. Bruggeman effective medium theory has been used by Knight et al. [14] to approximate the effective dielectric function of oxidized Al disks.

### 2.3. Maxwell Garnett (MG)

The Maxwell Garnett theory [6,12] considers the case of inclusions randomly spread in a continuous matrix. This theory is based on the Clausius–Mossotti relation, which relates the polarizability ( $\alpha$ ) with the dielectric function ( $\epsilon$ ). The effective dielectric function of a suspension of small spheres in a host material is given by

$$\frac{\epsilon_{eff} - \epsilon_h}{\epsilon_{eff} + 2\epsilon_h} = f \frac{\epsilon_I - \epsilon_h}{\epsilon_I + 2\epsilon_h}, \quad (3)$$

where  $\epsilon_h$  and  $\epsilon_I$  are the dielectric functions of host and inclusions materials, and  $f$  is the volume fraction of the embedded particles. Because a core-shell nanoparticle can be considered as an inclusion (core with dielectric function  $\epsilon_c$ ) in a host medium (shell with dielectric function  $\epsilon_s$ ) where  $\epsilon_I = \epsilon_c$  and  $\epsilon_h = \epsilon_s$ , its effective dielectric function can be expressed as

$$\epsilon_{eff} = \epsilon_s \frac{(\epsilon_c + 2\epsilon_s) + 2f(\epsilon_c - \epsilon_s)}{(\epsilon_c + 2\epsilon_s) - f(\epsilon_c - \epsilon_s)}. \quad (4)$$

Again,  $f$  is the filling factor that in the case of a spherical nano-shell is given by  $f = R_c^3/R_s^3$ . Notice that when  $f = 1$  (core-material particle)  $\epsilon_{eff} = \epsilon_c$ . On the contrary, when  $f = 0$  (shell-material particle)  $\epsilon_{eff} = \epsilon_s$ . Many authors have used this EMT to model the response of core-shell NPs [11,16,17].

### 2.4. Internal Homogenization (IH)

A more complex approach was introduced by Chettiar and Enghetta [15] through the concept of internal homogenization. Through this process the polarizability of the equivalent sphere is equated to that of a core-shell in the electrostatic approximation [12]. According to this, the effective dielectric function for a core-shell NP in vacuum is given by

$$\frac{\epsilon_{eff} - 1}{\epsilon_{eff} + 2} = \frac{(\epsilon_s - 1)(\epsilon_c + 2\epsilon_s) + f(\epsilon_c - \epsilon_s)(1 + 2\epsilon_s)}{(\epsilon_s + 2)(\epsilon_c + 2\epsilon_s) + 2f(\epsilon_s - 1)(\epsilon_c - \epsilon_s)}, \quad (5)$$

where  $f$  is the previously defined filling factor.

By rearranging Equation (5), the effective dielectric function can be expressed as the one given by an MG EMT, Equation (4), assuming a core embedded in a shell material medium with a filling factor of  $f$ . This equation that is independent of the particle size is only valid in the regime in which the size of the particle is much smaller than the incident wavelength (electrostatic approximation).

### 2.5. Mie Theory Based Maxwell Garnett (MMG)

A size dependent extension of the MG model, Equation (3), was proposed by Doyle [19,20] for a suspension of metallic spheres. In this case, the polarizability of the core embedded in shell material is given in terms of the Mie coefficient  $a_1$  [12] rather than the Clausius–Mossotti relation,

$$\frac{\epsilon_{eff} - \epsilon_s}{\epsilon_{eff} + 2\epsilon_s} = f \frac{3i}{2x^3} a_1. \quad (6)$$

This approach considers the size effects on the polarizability of the inclusion—core—in the host material—shell. In addition, by considering the polarizability of the core embedded in shell material, the validity of this model is restricted to the limit  $R_c \ll R_s$ .

### 3. New Approach

All the previous EMTs, already used in the literature, are either limited by the size of the particles (electrostatic approximation) or by the condition  $R_c \ll R_s$ . In this section, we present a new model aimed to overcome these limitations by considering the exact dipolar polarizability of the core-shell sphere in terms of the dipolar electric coefficient from the Mie expansion  $a_1^{cs}$ , and introducing radiating and depolarization effects in the polarizability of the effective sphere.

As stated above, we will first consider the exact polarizability of the core-shell nanoparticle ( $\alpha^{cs}$ ) in terms of its Mie dipolar electric coefficient  $a_1^{cs}$  [21],

$$\alpha^{cs} = \frac{3i}{2x^3} a_1^{cs}. \quad (7)$$

By doing this, size effects are being considered and the  $R_c \ll R_s$  condition is removed.

On the other hand, size effects in the effective dielectric function of the equivalent sphere can be taken into account by introducing dynamic depolarization and radiation damping factors [22]:

$$\alpha = \frac{\epsilon - 1}{(\epsilon + 2) - (\epsilon - 1)x^2 - (\epsilon - 1)(2i/3)x^3}, \quad (8)$$

where  $x$  is the size parameter given by  $x = 2\pi R/\lambda$  being  $R$  the size of the particle  $R = R_s$ . The depolarization factor considered here,  $(\epsilon - 1)x^2$ , is the one derived by Meier and Wokaun [22] by using a self-consistent derivation of the polarization of a sphere. It is worth mentioning that other expressions can be found for this factor in the literature calculated from a power-series expansion of the Mie coefficient  $a_1$ . For instance, Meier and Wokaun using a power expansion of the Mie coefficient obtained a depolarization factor of  $(\epsilon - 10/7)x^2$ . Other authors like Schebarchov et al. [23] and Tzarouchis et al. [24] through a Taylor and Padé expansions, respectively, have expressed this term scaling  $\propto (\epsilon - 2)x^2$ . Regarding the radiation damping,  $(\epsilon - 1)(2i/3)x^3$ , all authors have reported the same expression.

Thus, by considering the exact polarizability of the core-shell, Equation (7), and the depolarization and radiation damping factors in the polarizability of the equivalent sphere, Equation (8), we can express the effective dielectric function of an spherical nano-shell as

$$\frac{\epsilon_{eff} - 1}{(\epsilon_{eff} + 2) - (\epsilon_{eff} - 1)x^2 - (\epsilon_{eff} - 1)(2i/3)x^3} = \frac{3i}{2x^3} a_1^{cs}. \quad (9)$$

This approach is more of an internal homogenization process [15] than a Maxwell Garnett effective medium theory [19]. This new approach is a step forward in the methodology proposed by Chettiar and Engheta [15] given that our approach considers size effects in the polarizability of both effective sphere and coated sphere. For these reasons, from now on, we will refer to this proposed theory as Extended Internal Homogenization (Ext. IH).

### 4. Results

To evaluate the validity of the EMTs, we will compare the extinction efficiency spectra ( $Q_{ext}$ ) of metal-semiconductor core-shell spherical nanoparticles calculated with Mie theory for a coated sphere [12] (exact solution) with that obtained by using the effective dielectric function calculated

through each of the aforementioned EMTs in Mie theory for a homogeneous sphere [12]. For this study, we have chosen as plasmonic metal Au and three common semiconductors widely used in semiconductor photocatalysis:  $\text{Cu}_2\text{O}$ ,  $\text{CeO}_2$  and  $\text{TiO}_2$ . A broad variety of Au-core  $\text{Cu}_2\text{O}/\text{CeO}_2/\text{TiO}_2$ -shell nanoparticles have been reported in the literature for different photocatalytic applications [5,25,26]. A clear example of the utility of these core-shell nanostructures is the use Au- $\text{TiO}_2$  core-shell NPs in the water-splitting reaction. The efficient performance of this chemical reaction, in which water molecules dissociated into oxygen and hydrogen ( $2\text{H}_2\text{O} \rightarrow 2\text{H}_2 + \text{O}_2$ ), would have a great impact in the hydrogen economy [27]. Whereas  $\text{TiO}_2$  NPs can drive the water-splitting reaction by themselves when illuminated with UV light, when using Au- $\text{TiO}_2$ , the reaction can be driven by visible light, for instance that coming from the sun [28,29].

Figure 3 shows the dielectric function ( $\epsilon = \epsilon_r + i\epsilon_i$ ) of the chosen materials. The optical constants have been taken from different sources of the literature: Au [30],  $\text{Cu}_2\text{O}$  [31],  $\text{CeO}_2$  [32] and  $\text{TiO}_2$  [33].

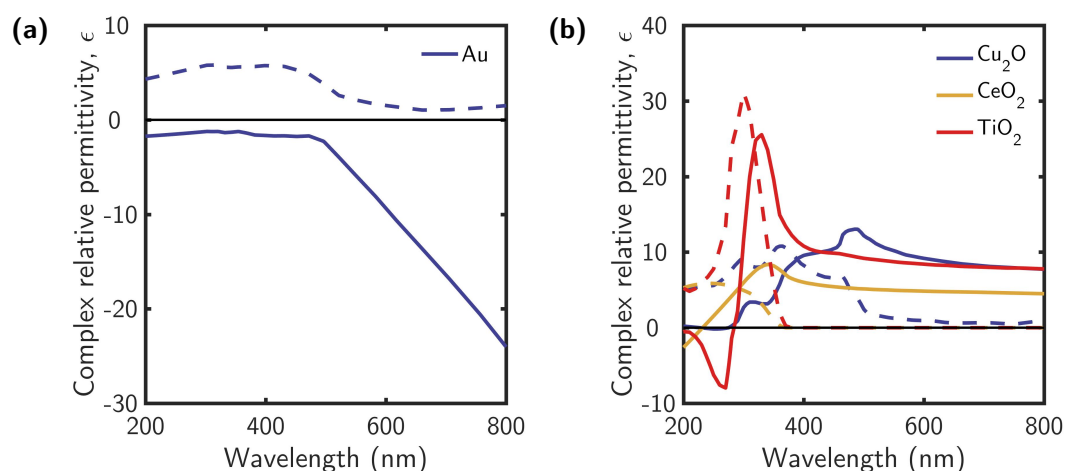


**Figure 3.** Complex dielectric function  $\epsilon = \epsilon_r + i\epsilon_i$  of (a) Au and (b)  $\text{Cu}_2\text{O}$  (blue),  $\text{CeO}_2$  (yellow) and  $\text{TiO}_2$  (red). The real  $\epsilon_r$  and imaginary part  $\epsilon_i$  of the complex dielectric function are plotted with solid and dashed lines, respectively. The optical constants have been taken from different sources of the literature: Au [30],  $\text{Cu}_2\text{O}$  [31],  $\text{CeO}_2$  [32] and  $\text{TiO}_2$  [33].

Figures 4–6 show the efficiency spectra ( $Q_{ext}$ ) of Au- $\text{CeO}_2$ , Au- $\text{Cu}_2\text{O}$  and Au- $\text{TiO}_2$  core-shell NPs with external radius  $R_s = 10, 20$  and  $30$  nm and varying core radii  $R_c$ . These sizes have chosen in order to work in the dipolar regime. The exact  $Q_{ext}$  spectra calculated with Mie theory for a coated sphere are compared with those obtained by using the effective dielectric functions in Mie theory for a homogeneous sphere. The considered effective dielectric functions have been calculated with the following EMTs: weighted average (WA), Bruggeman (Brugg), Maxwell Garnett (MG) (which leads to the same expression as the IH proposed by Chettiar–Enggheta), Mie theory based Maxwell Garnett (MMG) and the proposed approach (Ext. IH).

Figures 4–6 show that Maxwell Garnett (MG) and the proposed method (Ext. IH) give very similar results and both are the ones that better reproduce the exact solution given by Mie theory for a coated sphere. Conversely, Bruggeman EMT (Brug) is the one that worst describes the plasmonic response of the core-shell NPs. The reason arises from the basis of this theory i.e., both matrix and inclusions materials are interchangeable. In the system under study, interchanging the core and the shell materials lead to systems which, in principle, have a completely different plasmonic response. Those effective dielectric functions calculated by a weighted average EMT (WA) do not reproduce the exact solution. Although a plasmonic peak appears for the largest  $R_c$ , it is considerably blue-shifted and higher than those of the exact solution. The origin of these discrepancies comes from the construction of (1). When  $R_c \rightarrow 0$  (almost 100% shell material in the NP) and  $R_c \rightarrow R_s$  (almost 100% core material in the NP), it is expected to reach the convergence with the exact solution since  $\epsilon_{eff} \rightarrow \epsilon_s$  and  $\epsilon_{eff} \rightarrow \epsilon_c$ . However, for the intermediate values of  $R_c$ , and considering the high contrast of  $\epsilon_c$  (metallic material)

and  $\epsilon_s$  (dielectric material), the obtained average is far from that of the considered material because none of the underlying physics of the system are included in Equation (1). In the case of the Mie theory based Maxwell Garnett (MMG), although it presents a good agreement with small values of  $R_c$ , it fails to reproduce the values of  $Q_{ext}$ . All these problems emerge from the basis of this model. It considers the core embedded in an infinite matrix of shell material. When the metallic core is small, under illumination, the evanescent field exited by the LSPRs remains attached to it and dissipates within the dielectric shell. Therefore, the core can be considered to be completely embedded in shell material. However, as the shell thickness decreases, part of the evanescent field reaches beyond the outer shell surface. It is in this regime where MMG fails because the core cannot be considered to be hosted longer in an infinite shell [34]. In general, for all the EMTs under study, the predictions are worse as the size of the core-shell NP ( $R_s$ ) increases because quadrupolar effects start to emerge. For the same reason, the predictions are better for the smallest core sizes.

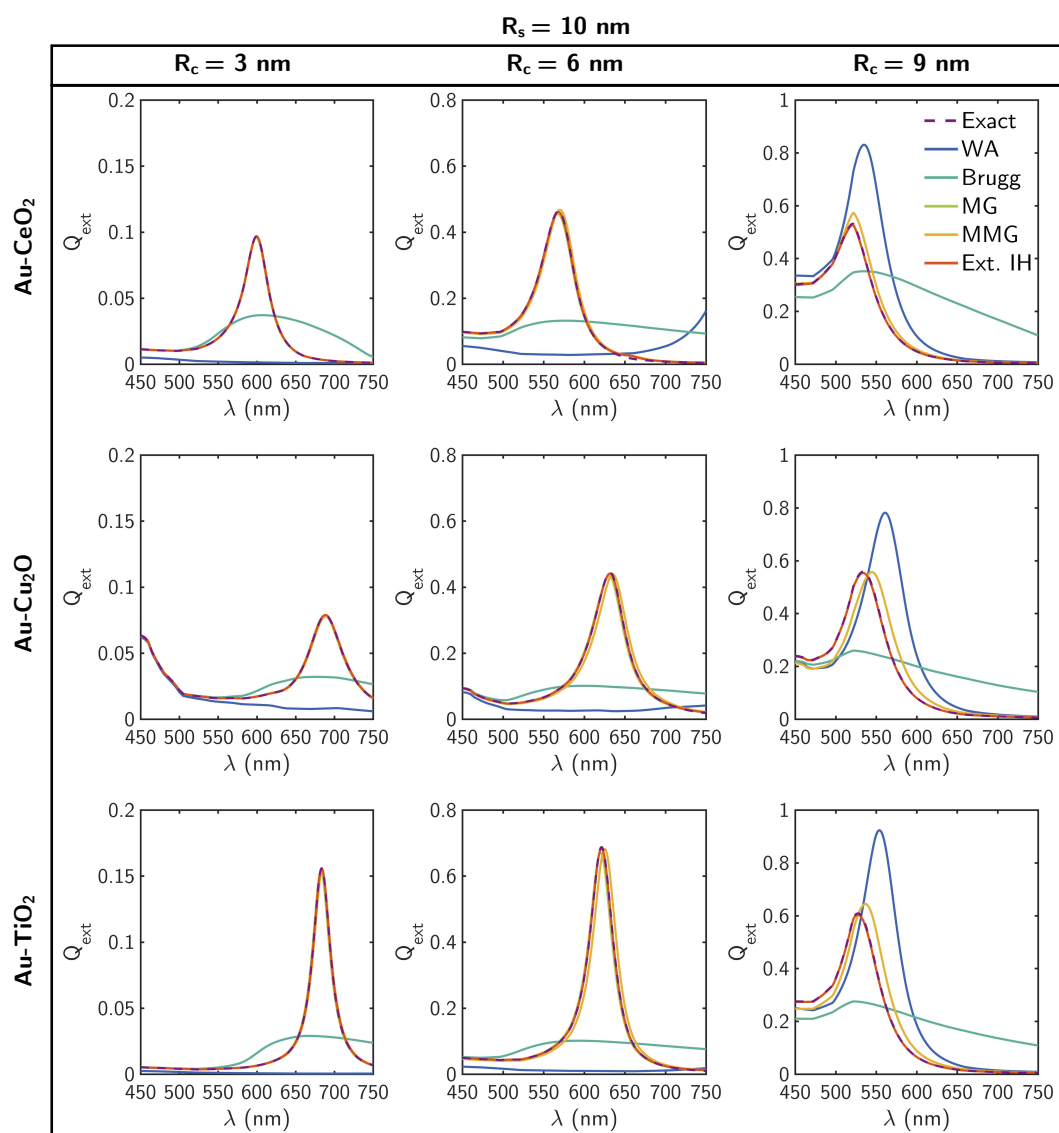


**Figure 4.** Extinction efficiency ( $Q_{ext}$ ) of Au-CeO<sub>2</sub> (top row), Au-Cu<sub>2</sub>O (middle row) and Au-TiO<sub>2</sub> (bottom row) core-shells of total radius  $R_s = 10$  nm and different core sizes:  $R_c = 3$  nm (first column),  $R_c = 6$  nm (middle column) and  $R_c = 9$  nm (right column). The exact solution is compared with different effective medium theories: weighted average (WA), Bruggeman (Brugg), Maxwell Garnett (MG), Mie theory based Maxwell Garnett (MMG) and the proposed approach (Ext. IH).

Since MG and Ext. IH EMTs fit the exact solution best, we have performed a more systematic comparison of the performance of both EMTs. For that reason, Figure 7 shows the spectral shift ( $\Delta\lambda$ , red right axis) of the  $Q_{ext}$  peak predicted through MG and Ext. IH EMTs with respect to the exact solution as a function of the core radius  $R_c$ . Indeed, the accurate prediction of the spectral position of the localized surface plasmon resonances is crucial in the design of core-shell nanoparticles for their application in photocatalysis. The precise selection of the resonant wavelength will determine the efficiency in which the catalyst absorbs light and the coupling of the enhanced electromagnetic field with the band gap of the semiconductor shell. Therefore, low values of  $\Delta\lambda$  are desirable. In addition, in Figure 7, the predicted values of the  $Q_{ext}$  peaks (blue left axis) along with the exact value are plotted. Again, Au-CeO<sub>2</sub> (top row), Au-Cu<sub>2</sub>O (middle row) and Au-TiO<sub>2</sub> core-shell NPs (bottom row) are considered. In this case, the total radii of the NPs are  $R_s = 15$  nm (left column),  $R_s = 25$  nm (middle column) and  $R_s = 35$  nm (right column). The calculations have been performed for core sizes ranging in  $2 \leq R_c \leq (R_s - 2)$  nm.

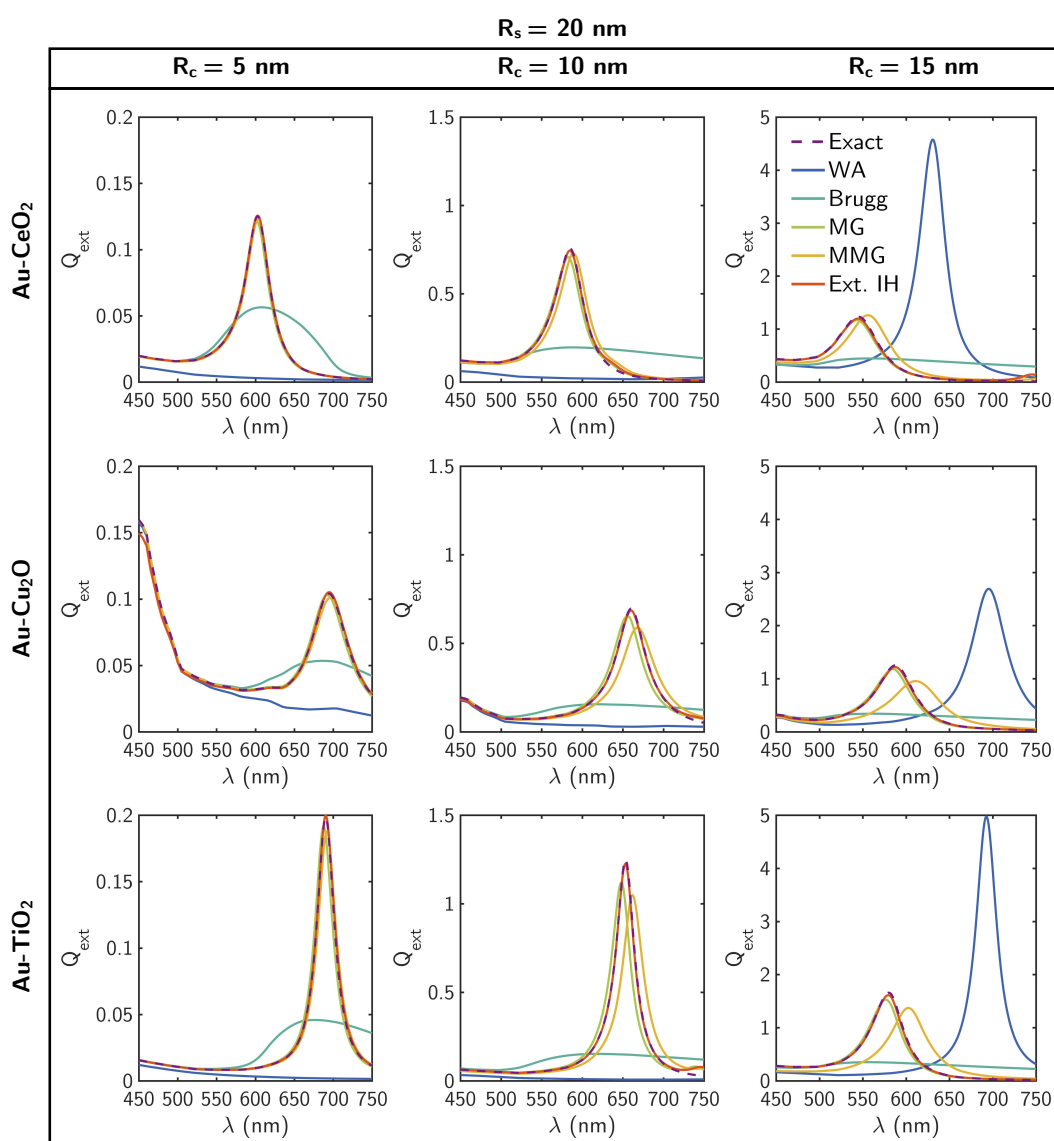


**Figure 5.** Extinction efficiency ( $Q_{ext}$ ) of Au-CeO<sub>2</sub> (top row), Au-Cu<sub>2</sub>O (middle row) and Au-TiO<sub>2</sub> (bottom row) core-shells of total radius  $R_s = 20$  nm and different core sizes:  $R_c = 5$  nm (first column),  $R_c = 10$  nm (middle column) and  $R_c = 15$  nm (right column). The exact solution is compared with different effective medium theories: weighted average (WA), Bruggeman (Brugg), Maxwell Garnett (MG), Mie theory based Maxwell Garnett (MMG) and the proposed approach (Ext. IH).



Concerning the values of the  $Q_{ext}$  peaks, the difference between the exact value and the predicted one increases as both the core and total radii become larger. Specifically, the predicted values are lower than the exact ones, those being given by Ext. IH closer to the exact solution. The only exception is produced for the largest  $R_c$  of the  $R_s = 25$  and  $35$  nm particles, where the value of MG is closer to that of Ext. IH. This is due to the fact that, for  $R_c \rightarrow R_s$ , the effective dielectric function  $\epsilon_{eff} \rightarrow \epsilon_s$  approaches the exact solution. This issue also appears when comparing the value of  $\Delta\lambda$  of both EMTs. In the case of MG, it can be seen how, for  $R_c \rightarrow R_s$  and  $R_c \rightarrow 0$ , the values are very close to that of the exact solution while the discrepancy is larger for intermediate values of  $R_c$ . On the contrary, for the Ext. IH,  $\Delta\lambda$  monotonically increases with the value of  $R_c$ . However, the values of  $\Delta\lambda$  are smaller than for MG in all the considered cases. For example, for  $R_s = 15$  and  $25$  nm,  $\Delta\lambda$  is always smaller than  $\approx 1$  nm while MG shows values of  $\Delta\lambda$  up to  $\approx 3$  and  $7.5$  nm, respectively. For the biggest NP size and the largest  $R_c$ , both MG and Ext. IH converge. However, for smaller values of  $R_c$ ,  $\Delta\lambda < 2.5$  nm for Ext. IH while for MG  $\Delta\lambda$  reaches up to  $15$  nm.

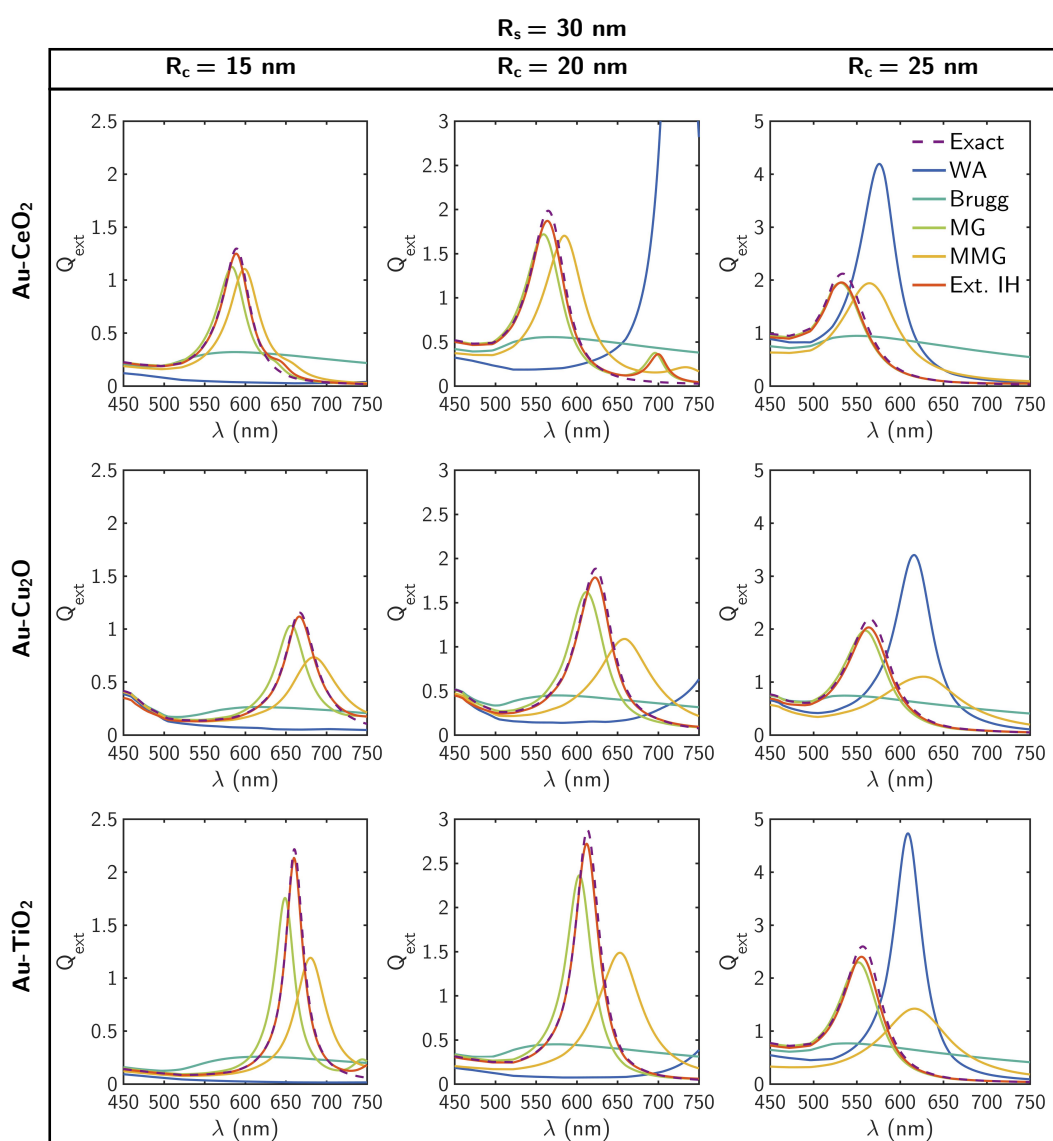


**Figure 6.** Extinction efficiency ( $Q_{ext}$ ) of Au-CeO<sub>2</sub> (top row), Au-Cu<sub>2</sub>O (middle row) and Au-TiO<sub>2</sub> (bottom row) core-shells of total radius  $R_s = 30$  nm and different core sizes:  $R_c = 15$  nm (first column),  $R_c = 20$  nm (middle column) and  $R_c = 25$  nm (right column). The exact solution is compared with different effective medium theories: weighted average (WA), Bruggeman (Brugg), Maxwell Garnett (MG), Mie theory based Maxwell Garnett (MMG) and the proposed approach (Ext. IH).

Therefore, taking into account all these results, we can conclude that the proposed approach shows a better performance in predicting the electromagnetic behavior of metal-semiconductor core-shells than conventional effective medium theories such as weighted average [13], Bruggeman [18], Maxwell Garnett [6] and Mie theory based Maxwell Garnett [20].

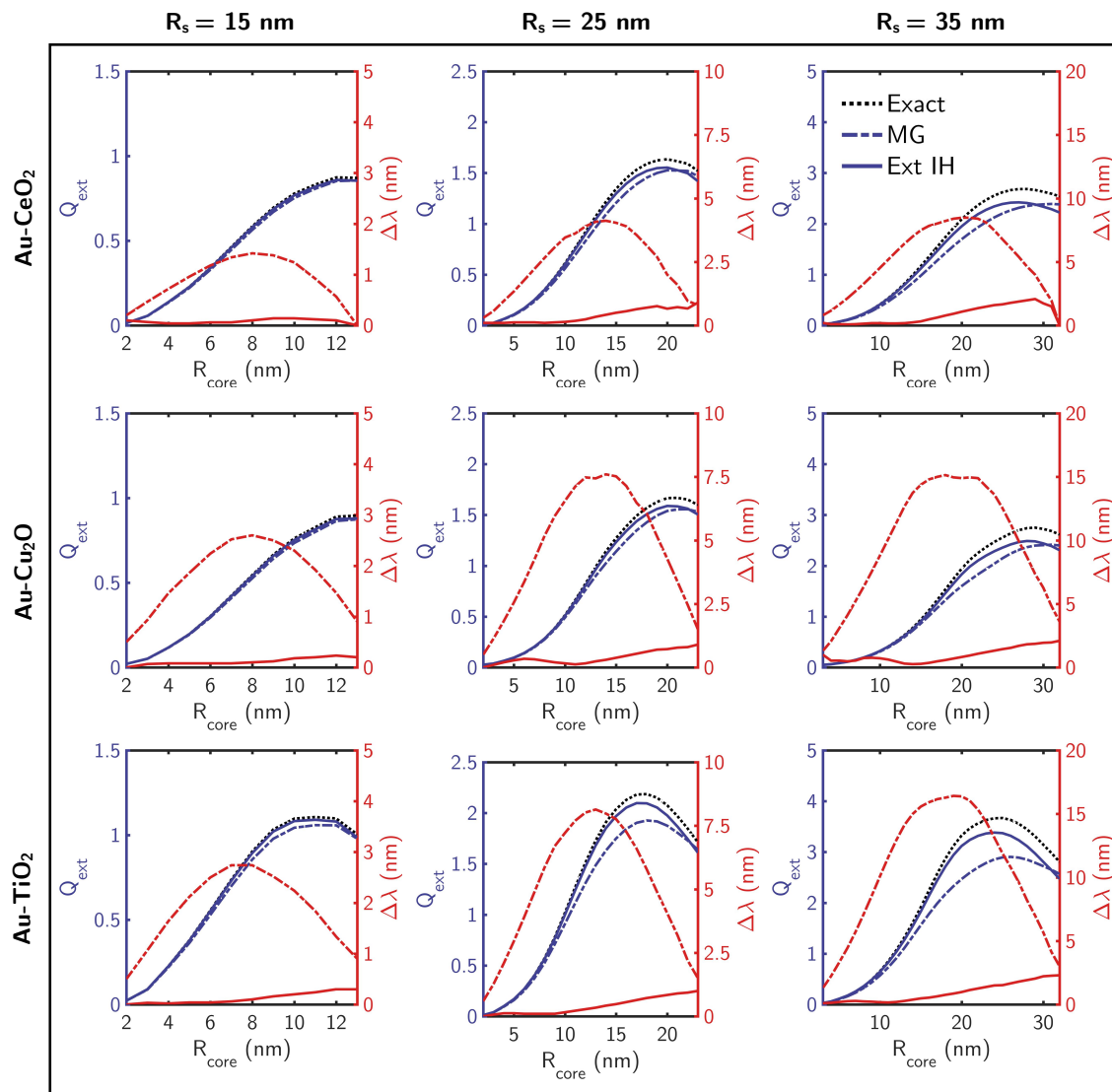


**Figure 7.** Value of the  $Q_{ext}$  peak (left blue axis) predicted by MG and Ext. IH, and their comparison with the exact solution. Spectral shift ( $\Delta\lambda$ , red right axis) of the  $Q_{ext}$  peak predicted through MG and Ext. IH effective medium theories (EMTs) with respect to the exact solution as a function of the core radius  $R_c$ . The nanoparticles considered are Au-CeO<sub>2</sub> (top row), Au-Cu<sub>2</sub>O (middle row) and Au-TiO<sub>2</sub> (bottom row) core-shells of total radius  $R_s$  and different core sizes:  $R_s = 15$  nm (first column),  $R_s = 25$  nm (middle column) and  $R_s = 35$  nm (right column).

## 5. Application: Reflectance of a Core-Shell Inclusion Type Composite

As an example of the applicability of the results in this research, here we will compare the reflectance at normal incidence of a system consisting of a homogeneous slab with metal-semiconductor core-shell inclusions calculated using different methods. The slab (i.e., host medium) has been considered to have a thickness of  $h = 60$  nm and a dielectric function  $\epsilon_h = 1.77$  (water). The core-shell inclusions have an Au core of radius  $R_c = 10$  nm, and the shell has a thickness of 10 nm and dielectric function  $\epsilon_s = 9$  (TiO<sub>2</sub>). The filling fraction of inclusions in the slab is  $f = 0.17$ . A scheme of this system is sketched

in Figure 8a. Note that there is not an analytical solution to calculate the reflectance of these types of systems.

The reflectances have been calculated using three different methodologies:

- Using FDTD Lumerical software (Lumerical Inc., Vancouver, Canada) (numerical solution of Maxwell's equations), we have built a unit cell periodically replicated in the plane perpendicular to the wave vector of the illuminating beam ( $\mathbf{k}$  in Figure 8a) that reproduces the characteristics of the system under study.
- Using the Transfer Matrix Method [35] taking as inputs the effective dielectric constant of the slab with the core-shell inclusions and its thickness ( $h = 60$  nm). The procedure followed is illustrated in Figure 9. (i) The initial system is reduced to one in which the core-shell inclusions are transformed into homogeneous spheres with dielectric function  $\epsilon_{cs}$ . The dielectric function of these homogeneous spheres ( $\epsilon_{cs}$ ) has been calculated following the proposed approach (Equation (9)). (ii) Using Maxwell Garnett, taking as inputs the dielectric function of the host medium (water,  $\epsilon_h = 1.77$ ), the effective dielectric function of the inclusions calculated using Equation (9) ( $\epsilon_{cs}$ ), and the filling fraction ( $f = 0.17$ ), we have calculated the effective medium of the whole system  $\epsilon_{eff}$ . Finally, using the Transfer Matrix Method (TMM) [35], we have calculated the reflectance of a homogeneous slab with dielectric function  $\epsilon_{eff}$  and thickness  $h = 60$  nm at normal incidence.
- Following the same recipe of the previous point, but, instead of using the proposed approach to calculate the effective dielectric function of the core-shell with Equation (9), we have used Maxwell Garnett (Equation (4)), a widely used approach to model core-shell NPs [11,16,17]. This EMT has shown the second best performance in our study. It is worth mentioning that this equation is equivalent to that proposed by Chettiar–Engchetta for the internal homogenization of coated spheres (Equation (5)) [15].

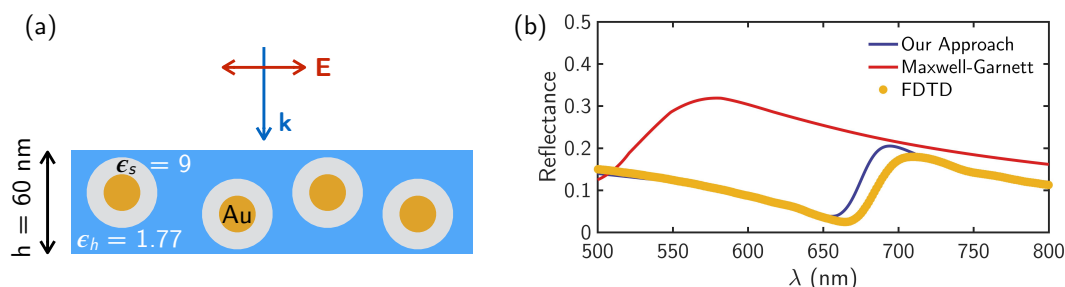


**Figure 8.** (a) scheme of the system under study: an slab (i.e., host medium) with constant real dielectric function  $\epsilon_h = 1.77$  with core-shell inclusions ( $R_c = 10$  nm and  $R_s = 20$  nm). The core is made of Au and the shell has a constant real dielectric function of  $\epsilon_s = 9$ . The system is illuminated under normal incidence ( $\mathbf{k}$ ) with a linear polarized wave ( $\mathbf{E}$ ); (b) reflectance calculations on the system in sketched in (a). Yellow dots represent the numerical solution of the reflectance given by FDTD simulations. The reflectance calculated using the Transfer Matrix Method [35] in a system like that of Figure 9 is plotted: using in step (i) the proposed approach (blue line) and Maxwell Garnett (red line), and in step (ii) Maxwell Garnett.

The result of this comparison is shown in Figure 8b. Yellow dots represent the numerical solution given by the FDTD simulations. The reflectances obtained by TMM using the proposed approach and Maxwell Garnett to calculate the effective dielectric function of the inclusions are represented in blue and red, respectively. The numerical solution presents a characteristic dip at 663 nm. While using Maxwell Garnett to calculate the effective dielectric function of the core-shell completely fails to reproduce this dip, our approach clearly reproduces it. More precisely, in the latter case, the dip is produced at 657 nm (showing a 5 nm deviation from the numerical solution). The discrepancy between the exact solution and that derived by using our approach to calculate the effective dielectric function of the inclusion as input for the Maxwell Garnett of the composite comes from the fact that

Maxwell-Garnett assumes inclusions in the dipolar regime. As the size of the inclusions increases, and high order multipoles start to contribute, the inaccuracy of the effective dielectric function also increases. This size effects are enhanced when the particles are surrounded by a medium denser than vacuum since the wavelength inside the host matrix is shorter, making the particle effectively bigger. Therefore, by using our proposed approach, we can get a very good estimation of the reflectance on this type of systems without the need for using advanced electromagnetic simulations software.



**Figure 9.** Procedure to reduce a system consisting on a composite core-shell type inclusion into a homogeneous slab.

## 6. Conclusions

In this work, we propose a new approach to calculate the effective dielectric function of metal-semiconductor core-shell spherical NPs. Basically, this new method works by introducing radiating and depolarizing effects in the polarizability of the effective sphere, and considering the exact polarizability of the core-shell constructed from the dipolar electric Mie scattering coefficient. This new approach has shown a better performance than the current EMTs for metal-semiconductor core-shell NPs, especially in the prediction of the spectral position of the localized surface plasmon resonances i.e., a key parameter in the design of efficient photocatalysts. While the weighted average and Bruggeman EMTs completely fail to predict the plasmonic response of the metal-semiconductor nano-shells, Mie Maxwell Garnett show a good performance for the smallest core sizes. Maxwell Garnett and the proposed approach are the ones that better reproduce the exact solution. Although Maxwell Garnett EMT reproduces the exact solution when  $R_c \rightarrow 0$  and  $R_c \rightarrow R_s$  well, for intermediate values of  $R_c$ , the proposed approach shows a better performance. We believe that this method can be helpful for predicting the reflectance, transmittance, and absorptance spectra, and engineering the effective permittivity of composites and colloids with core-shell type inclusions used in photocatalysis and solar energy harvesting.

**Author Contributions:** Y.G. wrote the paper and performed the numerical calculations. All authors analyzed the results and figures. F.G. and F.M. supervised the study.

**Funding:** This research was funded by the Army Research Laboratory under Cooperative Agreement Number W911NF-17-2-0023 and by SODERCAN (Sociedad para el Desarrollo de Cantabria) and the Research Vicerrectorate of the University of Cantabria through project 4JU2864661.

**Acknowledgments:** Y.G. acknowledges the University of Cantabria for her FPU grant.

**Conflicts of Interest:** The authors declare no conflict of interest.

## References

1. Tong, H.; Ouyang, S.; Bi, Y.; Umezawa, N.; Oshikiri, M.; Ye, J. Nano-photocatalytic materials: Possibilities and challenges. *Adv. Mater.* **2012**, *24*, 229–251. [[CrossRef](#)] [[PubMed](#)]
2. Zhang, X.; Chen, Y.L.; Liu, R.S.; Tsai, D.P. Plasmonic photocatalysis. *Rep. Prog. Phys. Phys. Soc.* **2013**, *76*, 046401. [[CrossRef](#)] [[PubMed](#)]
3. Hou, W.; Cronin, S.B. A review of surface plasmon resonance-enhanced photocatalysis. *Adv. Funct. Mater.* **2013**, *23*, 1612–1619. [[CrossRef](#)]
4. Ma, L.; Chen, S.; Shao, Y.; Chen, Y.L.; Liu, M.X.; Li, H.X.; Mao, Y.L.; Ding, S.J. Recent Progress in Constructing Plasmonic Metal/Semiconductor Hetero-Nanostructures for Improved Photocatalysis. *Catalysts* **2018**, *8*, 634. [[CrossRef](#)]
5. Wang, P.; Huang, B.; Dai, Y.; Whangbo, M.H. Plasmonic photocatalysts: harvesting visible light with noble metal nanoparticles. *Phys. Chem. Chem. Phys.* **2012**, *14*, 9813. [[CrossRef](#)] [[PubMed](#)]

6. Maxwell Garnett, J.C. Colours in Metal Glasses, in Metallic Films, and in Metallic Solutions II. *Philos. Trans. R. Soc. A Math. Phys. Eng. Sci.* **1906**, *205*, 237–288. [[CrossRef](#)]
7. Sihvola, A. *Electromagnetic Mixing Formulas and Applications*; IET, The Institution of Engineering and Technology, Michael Faraday House: Stevenage, UK, 1999. [[CrossRef](#)]
8. Milton, G.W. *The Theory of Composites*; Cambridge University Press: Cambridge, UK, 2002. [[CrossRef](#)]
9. Pathak, N.K.; Chander, N.; Komarala, V.K.; Sharma, R.P. Plasmonic Perovskite Solar Cells Utilizing Au@SiO<sub>2</sub> Core-Shell Nanoparticles. *Plasmonics* **2016**, *12*, 1–8. [[CrossRef](#)]
10. Zhang, W.; Saliba, M.; Stranks, S.D.; Sun, Y.; Shi, X.; Wiesner, U.; Snaith, H.J. Enhancement of Perovskite-Based Solar Cells Employing Core-Shell Metal Nanoparticles. *Nano Lett.* **2013**, *13*, 4505–4510. [[CrossRef](#)]
11. Taylor, R.A.; Phelan, P.E.; Otanicar, T.P.; Lv, W.; Swaminathan, R. Multifunctional Core-Shell Nanoparticle Suspensions for Efficient Absorption. *J. Sol. Energy Eng.* **2012**, *135*, 021004. [[CrossRef](#)]
12. Bohren, C.F.; Huffman, D.R. (Eds) *Absorption and Scattering of Light by Small Particles*; Wiley-VCH Verlag GmbH: Weinheim, Germany, 1998. [[CrossRef](#)]
13. Kuzma, A.; Weis, M.; Flickyngeroova, S.; Jakabovic, J.; Satka, A.; Dobrocka, E.; Chlpik, J.; Cirak, J.; Donoval, M.; Telek, P.; et al. Influence of surface oxidation on plasmon resonance in monolayer of gold and silver nanoparticles. *J. Appl. Phys.* **2012**, *112*, 103531. [[CrossRef](#)]
14. Knight, M.W.; King, N.S.; Liu, L.; Everitt, H.O.; Nordlander, P.; Halas, N.J. Aluminum for plasmonics. *ACS Nano* **2014**, *8*, 834–840. [[CrossRef](#)] [[PubMed](#)]
15. Chettiar, U.K.; Engheta, N. Internal homogenization: Effective permittivity of a coated sphere. *Opt. Exp.* **2012**, *20*, 22976. [[CrossRef](#)] [[PubMed](#)]
16. Li, S.Y.; Niklasson, G.A.; Granqvist, C.G. Nanothermochromics with VO<sub>2</sub>-based core-shell structures: Calculated luminous and solar optical properties. *J. Appl. Phys.* **2011**, *109*, 113515. [[CrossRef](#)]
17. Li, J.; Sun, G.; Chan, C.T. Optical properties of photonic crystals composed of metal-coated spheres. *Phys. Rev. B Cond. Matter Mater. Phys.* **2006**, *73*, 1–10. [[CrossRef](#)]
18. Bruggeman, D.A.G. Berechnung verschiedener physikalischer Konstanten von heterogenen Substanzen. I. Dielektrizitätskonstanten und Leitfähigkeiten der Mischkörper aus isotropen Substanzen. *Ann. Phys.* **1935**, *416*, 636–664. [[CrossRef](#)]
19. Doyle, W.T. Optical properties of a suspension of metal spheres. *Phys. Rev. B* **1989**, *39*, 9852–9858. [[CrossRef](#)]
20. Ruppin, R. Evaluation of extended Maxwell-Garnett theories. *Opt. Commun.* **2000**, *182*, 273–279. [[CrossRef](#)]
21. Mulholland, G.W.; Bohren, C.F.; Fuller, K.a. Light Scattering by Agglomerates: Coupled Electric and Magnetic Dipole Method. *Langmuir* **1994**, *10*, 2533–2546. [[CrossRef](#)]
22. Meier, M.; Wokaun, A. Enhanced fields on large metal particles: dynamic depolarization. *Opt. Lett.* **1983**, *8*, 581–583. [[CrossRef](#)] [[PubMed](#)]
23. Schebarchov, D.; Auguié, B.; Le Ru, E.C. Simple accurate approximations for the optical properties of metallic nanospheres and nanoshells. *Phys. Chem. Chem. Phys. PCCP* **2013**, *15*, 4233–4242. [[CrossRef](#)]
24. Tzarouchis, D.C.; Ylä-Oijala, P.; Sihvola, A. Unveiling the scattering behavior of small spheres. *Phys. Rev. B* **2016**, *94*, 140301. [[CrossRef](#)]
25. Mondal, K.; Moitra, P. Metal-semiconductor core-shell nanostructured photocatalysts for environmental applications and their recycling process. In *Metal Semiconductor Core-Shell Nanostructures for Energy and Environmental Applications*; Number 1; Elsevier: Amsterdam, The Netherlands, 2017; pp. 133–157. [[CrossRef](#)]
26. Li, J.; Cushing, S.K.; Bright, J.; Meng, F.; Senty, T.R.; Zheng, P.; Bristow, A.D.; Wu, N. Ag@Cu<sub>2</sub>O Core-Shell Nanoparticles as Visible-Light Plasmonic Photocatalysts. *ACS Catal.* **2013**, *3*, 47–51. [[CrossRef](#)]
27. Schlapbach, L.; Züttel, A. Hydrogen-storage materials for mobile applications. *Nature* **2001**, *414*, 353–358. [[CrossRef](#)] [[PubMed](#)]
28. Gomes Silva, C.; Juarez, R.; Marino, T.; Molinari, R.; Garcia, H. Influence of Excitation Wavelength (UV or Visible Light) on the Photocatalytic Activity of Titania Containing Gold Nanoparticles for the Generation of Hydrogen or Oxygen from Water. *J. Am. Chem. Soc.* **2011**, *133*, 595–602. [[CrossRef](#)] [[PubMed](#)]
29. Linic, S.; Christopher, P.; Ingram, D.B. Plasmonic-metal nanostructures for efficient conversion of solar to chemical energy. *Nat. Mater.* **2011**, *10*, 911–921. [[CrossRef](#)] [[PubMed](#)]
30. Palik, E.D. *Handbook of Optical Constants of Solids*; Academic Press: Cambridge, MA, USA, 1998.
31. Ito, T.; Yamaguchi, H.; Masumi, T.; Adachi, S. Optical Properties of CuO Studied by Spectroscopic Ellipsometry. *J. Phys. Soc. Jpn.* **1998**, *67*, 3304–3309. [[CrossRef](#)]

32. Shih, W.C.; Chen, C.H.; Chiu, F.C.; Lai, C.M.; Hwang, H. CeO<sub>2</sub> optical properties and electrical characteristics. *ECS Trans.* **2010**, *28*, 435–442. [[CrossRef](#)]
33. Devore, J.R. Refractive Indices of Rutile and Sphalerite. *J. Opt. Soc. Am.* **1951**, *41*, 416. [[CrossRef](#)]
34. Gutierrez, Y.; Ortiz, D.; Sanz, J.M.; Saiz, J.M.; Gonzalez, F.; Everitt, H.O.; Moreno, F. How an oxide shell affects the ultraviolet plasmonic behavior of Ga, Mg, and Al nanostructures. *Opt. Exp.* **2016**, *24*, 20621. [[CrossRef](#)]
35. Born, M.; Wolf, E.; Bhatia, A.B.; Clemmow, P.C.; Gabor, D.; Stokes, A.R.; Taylor, A.M.; Wayman, P.A.; Wilcock, W.L. *Principles of Optics*; Cambridge University Press: Cambridge, UK, 1999. [[CrossRef](#)]



© 2019 by the authors. Licensee MDPI, Basel, Switzerland. This article is an open access article distributed under the terms and conditions of the Creative Commons Attribution (CC BY) license (<http://creativecommons.org/licenses/by/4.0/>).